

Designing thermal demultiplexer: Splitting phonons by negative mass and genetic algorithm optimization

Yu-Tao Tan(谭宇涛), Lu-Qin Wang(王鲁钦), Zi Wang(王子), Jiebin Peng(彭洁彬), and Jie Ren(任捷)

Citation: Chin. Phys. B, 2021, 30 (**3**): 036301. DOI: 10.1088/1674-1056/abd68b
Journal homepage: http://cpb.iphy.ac.cn; http://iopscience.iop.org/cpb

What follows is a list of articles you may be interested in

Raman scattering from highly-stressed anvil diamond

Shan Liu(刘珊), Qiqi Tang(唐琦琪), Binbin Wu(吴彬彬), Feng Zhang(张峰), Jingyi Liu(刘静仪), Chunmei Fan(范春梅), and Li Lei(雷力)

Chin. Phys. B, 2021, 30 (**1**): 016301. DOI: 10.1088/1674-1056/abc7a7

Acoustic topological phase transition induced by band inversion of high-order compound modes and robust pseudospin-dependent transport

Yan Li(李妍)†, Yi-Nuo Liu(刘一诺), and Xia Zhang(张霞)

Chin. Phys. B, 2020, 29 (**10**): 106301. DOI: 10.1088/1674-1056/abad21

Raman scattering study of two-dimensional magnetic van der Waals compound VI_3

Yi-Meng Wang(王艺朦), Shang-Jie Tian(田尚杰), Cheng-He Li(李承贺), Feng Jin(金峰), Jian-Ting Ji(籍建亭), He-Chang Lei(雷和畅), Qing-Ming Zhang(张清明)

Chin. Phys. B, 2020, 29 (**5**): 056301. DOI: 10.1088/1674-1056/ab8215

Material properties dependent on the thermal transport in a cylindrical nanowire

Zhang Yong, Xie Zhong-Xiang, Deng Yuan-Xiang, Yu Xia, Li Ke-Min

Chin. Phys. B, 2015, 24 (**12**): 126302. DOI: 10.1088/1674-1056/24/12/126302

Thermal conductance in a two-slit quantum waveguide

Nie Liu-Ying,Li Chun-Xian,Zhou Xiao-Ping,Wang Cheng-Zhi,Cheng Fang

Chin. Phys. B, 2012, 21 (**2**): 026301. DOI: 10.1088/1674-1056/21/2/026301

SPECIAL TOPIC — Phononics and phonon engineering

Designing thermal demultiplexer: Splitting phonons by negative mass and genetic algorithm optimization*

Yu-Tao Tan(谭宇涛)[1], Lu-Qin Wang(王鲁钦)[1,†], Zi Wang(王子)[1], Jiebin Peng(彭洁彬)[1], and Jie Ren(任捷)[1,2,‡]

[1] *Center for Phononics and Thermal Energy Science, China-EU Joint Laboratory on Nanophononics, Shanghai Key Laboratory of Special Artificial Microstructure Materials and Technology, School of Physics Science and Engineering, Tongji University, Shanghai* 200092, *China*

[2] *Shanghai Research Institute for Intelligent Autonomous Systems, Tongji University, Shanghai* 200092, *China*

(Received 1 October 2020; revised manuscript received 13 December 2020; accepted manuscript online 24 December 2020)

We propose the concept of thermal demultiplexer, which can split the heat flux in different frequency ranges into different directions. We demonstrate this device concept in a honeycomb lattice with dangling atoms. From the view of effective negative mass, we give a qualitative explanation of how the dangling atoms change the original transport property. We first design a two-mass configuration thermal demultiplexer, and find that the heat flux can flow into different ports in corresponding frequency ranges roughly. Then, to improve the performance, we choose the suitable masses of dangling atoms and optimize the four-mass configuration with genetic algorithm. Finally, we give out the optimal configuration with a remarkable effect. Our study finds a way to selectively split spectrum-resolved heat to different ports as phonon splitter, which would provide a new means to manipulate phonons and heat, and to guide the design of phononic thermal devices in the future.

Keywords: phonon transport, thermal demultiplexer, optimization algorithm

PACS: 63.20.−e, 63.20.Pw, 63.22.−m, 05.70.Ln **DOI:** 10.1088/1674-1056/abd68b

1. Introduction

Manipulating heat transport and understanding the mechanism are long-standing goals in both classical and quantum open systems.[1] Conventionally, many studies have presented phonon transport manipulation in different systems such as aperiodic lattice,[2,3] composite material,[4] porous system,[5] graphene folding[6,7] isotopic doping,[8,9] disorder system,[10,11] edge roughness,[12] and so on. Furthermore, in analogy to the modern electronics, many thermal functional devices have been realized theoretically, including the thermal diode,[13,14] the thermal transistor,[15,16] the thermal memory,[17,18] the thermal capacitor,[20] and even the thermal logical gate for computing.[19] Moreover, many experiments have realized these thermal operations.[21–23]

In phononic thermal transport, people usually integrate the whole phonon frequency range when calculating heat flux and thermal conductivity, because all spectra contribute to thermal transport. Yet, there is lack of exploration of controlling the spectrum-resolved phonon transport at the different frequencies and wavelengths. Managing different phonon transport of different frequencies can largely broaden the scope of applications of phononic devices, which is able to achieve the spectrum-resolved manipulations of thermal and phonon transport, as the multiplexer and demultiplexer in phononics. For example, dielectric wavelength (frequency) demultiplexer has been demonstrated in integrated photonic devices.[24,25] This frequency-dependent demultiplexer will split the light, which means the short wavelength (high frequency) light will transmit to one port while the long wavelength (low frequency) light will transmit to the other. Similarly, there exist both theoretical and experimental proposals for acoustic demultiplexer by exploiting sonic crystals.[26–28]

In this work, we design a thermal demultiplexer that will split phonons of different frequency ranges and transmit them to different ports. Concretely, in Section 2 we first introduce the dangling atoms model, which is shown in Fig. 1(a). Dangling atoms will lead to zero transmission in specific frequency range, which can be explained by the concept of negative mass.[29–33] Then we show how to calculate the transmission and heat flux via the nonequilibrium Green's function (NEGF) method.[34–37] In Section 3, we start with a thermal demultiplexer with two-mass dangling atoms that can split the phonons into different ports with different frequency ranges. We then use genetic algorithm (GA) to optimize the structure for a better demultiplexer performance. Finally, we conclude in Section 4.

*Project supported by the National Natural Science Foundation of China (Grant Nos. 11935010 and 11775159), the Shanghai Science and Technology Committee, China (Grant Nos. 18ZR1442800 and 18JC1410900), and the Opening Project of Shanghai Key Laboratory of Special Artificial Microstructure Materials and Technology.

†Corresponding author. E-mail: Rick_wanglq@163.com

‡Corresponding author. E-mail: Xonics@tongji.edu.cn

© 2021 Chinese Physical Society and IOP Publishing Ltd

2. Structure and method

The primary structure we used in this paper is the infinite honeycomb lattice. But each atom connects to an extra atom, namely, the dangling atom, whose schematic view is shown in Fig. 1(a).

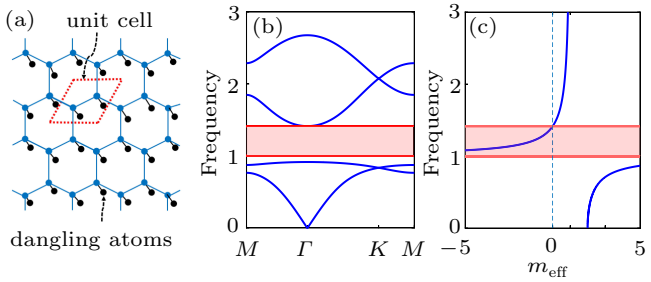


Fig. 1. (a) Schematic view of infinite honeycomb lattice with dangling atoms and the unit cell is shown in red dashed parallelogram. (b) Dispersion relation of infinite honeycomb lattice with dangling atoms. (c) Effective mass versus frequency. The pink shadow region denotes the effective negative mass zone. The frequency gap of the dispersion relation almost coincides with the effective negative mass zone.

To understand how the dangling atoms affect phonon transport, we calculate the dispersion relation of the honeycomb lattice with dangling atoms shown in Fig. 1(b). In our calculation, we set lattice atoms' mass $m_0 = 1$, dangling atoms' mass $m_{\rm d} = 1$, the coupling constant $k_{\rm d} = 1$ between them, and the inner coupling constant of lattice atoms $k_0 = 1$. Here without loss of generality, we consider scalar phonon model, i.e., only one-dimensional vibration, the scalar displacement from each atom's equilibrium position, is taken into account. After Fourier transformation, the equation of motion is described as

$$-\omega^2 \boldsymbol{M}\boldsymbol{X}_{\boldsymbol{k}} = \boldsymbol{K}\boldsymbol{X}_{\boldsymbol{k}}. \tag{1}$$

The dynamical matrix $\boldsymbol{K}$ is described as

$$\boldsymbol{K} = \begin{pmatrix} -3k_0 - k_1 & k_1 & k_0\Phi & 0 \\ k_1 & -k_1 & 0 & 0 \\ k_0\Phi^* & 0 & -3k_0 - k_1 & k_1 \\ 0 & 0 & k_1 & -k_1 \end{pmatrix}, \tag{2}$$

where $\Phi = 1 + \mathrm{e}^{\mathrm{i}(\frac{\sqrt{3}}{2}k_x + \frac{3}{2}k_y)} + \mathrm{e}^{\mathrm{i}(-\frac{\sqrt{3}}{2}k_x + \frac{3}{2}k_y)}$, Φ^* is the complex conjugate, and $\boldsymbol{M} = \mathrm{diag}\{m_0, m_1, m_0, m_1\}$. Obviously, the band gap induced by dangling atoms is opened which will cause the specific phonon transport forbidden. This is the key ingredient to design the thermal demultiplexer.

To describe the collective behavior of lattice atoms and dangling atoms, we introduce the effective mass term. For the effective mass $m_{\rm eff}$, it can be calculated by

$$m_{\rm eff} = m_0 + \frac{k_{\rm d} m_{\rm d}}{k_{\rm d} - m_{\rm d}\omega^2}. \tag{3}$$

Here $m_{\rm eff}$ is a function of frequency ω.[32,33]

In phononic metamaterial, effective negative parameters, which means some effective parameters will become negative at some frequency range, have been thoroughly studied.[29–31] The mass–spring structure[32] is a common used system to realize effective negative parameters. Interestingly, effective negative parameters may contribute to zero transmission.[33] In our system, the effective negative mass (ENM) frequency range is given by

$$\sqrt{\frac{k_{\rm d}}{m_{\rm d}}} < \omega < \sqrt{\frac{k_{\rm d}}{m_{\rm d}}\left(\frac{m_0 + m_{\rm d}}{m_0}\right)}. \tag{4}$$

In Fig. 1(c), we not only show the effective mass curve but also mark the ENM zone by the pink shadow zone. In the frequency range of ENM, original propagating modes will become localized or resonant modes which contribute to the frequency gap that phonon cannot transport. As we expect, the ENM region matches with the band gap very well.

From the dispersion relation, we can see that the upper boundary frequency of ENM and band gap are equal while there is tiny difference between two lower boundaries. This is mainly because the effective mass works well in long wave limit Γ point but poorly on the border of Brillouin zone M point due to Bragg scattering. The two upper boundaries match well because the minimum value of optical branches (two upper branches) are at Γ point. However, it seems that the maximum values of acoustic branches (two lower branches) are also at Γ point, mainly because of the band fold. The maximum value of acoustic branch was originally on the border of the Brillouin zone but after the band folding it turns to the Γ point.

We propose a three-port demultiplexer whose diagram is shown in Fig. 2(a). The structure is a finite honeycomb lattice with dangling atoms and connects with three ports which are Langevin heat baths. We then use NEGF method to calculate transmission and heat flux.[34,37] First of all, we set the displacement vector and momentum vector as $\boldsymbol{X} = \{x_1, x_2, \ldots, x_N\}^{\rm T}$ and $\boldsymbol{P} = \{p_1, p_2, \ldots, p_N\}^{\rm T}$, then the Hamiltonian of this system can be expressed as

$$H = \frac{1}{2}\boldsymbol{P}^{\rm T}\boldsymbol{M}^{-1}\boldsymbol{P} + \frac{1}{2}\boldsymbol{X}^{\rm T}\boldsymbol{K}\boldsymbol{X}, \tag{5}$$

where $\boldsymbol{M}$ is the mass matrix and $\boldsymbol{K}$ is the coupling matrix. Then the retarded Green's function $G^{\rm r}(\omega)$ for a common two-port setup is given out

$$G^{\rm r}(\omega) = \frac{1}{-\omega^2\boldsymbol{M} + \boldsymbol{K} - \Sigma_{\rm L}^{+}(\omega) - \Sigma_{\rm R}^{+}(\omega)}, \tag{6}$$

where $\Sigma_{\rm L}^{+}(\omega)$ and $\Sigma_{\rm R}^{+}(\omega)$ are self-energy of heat bath in the left and right. After getting the $G^{\rm r}(\omega)$, the transmission $\mathcal{T}(\omega)$ can be expressed as

$$\mathcal{T}(\omega) = 4\mathrm{Tr}[G^{\rm r}(\omega)\Gamma_{\rm L}(\omega)G^{\rm a}(\omega)\Gamma_{\rm R}(\omega)], \tag{7}$$

where $G^{\rm a}(\omega) = G^{\rm r}(\omega)^{\dagger}$ and $\Gamma(\omega) = \mathrm{Im}[\Sigma(\omega)]$. Choosing the Σ^{+} corresponding to each port, we can calculate the phonon's transmission from the input port to one output port. We can also calculate the correlation C between displacement $\boldsymbol{X}$ and

velocity $\dot{\boldsymbol{X}}$

$$C = \langle \boldsymbol{X}\dot{\boldsymbol{X}}^{\mathrm{T}} \rangle = \frac{2k_{\mathrm{B}}T_{\mathrm{L}}}{\pi}\int_0^{\infty} \mathrm{d}\omega\omega G^{\mathrm{r}}(\omega)\Gamma_{\mathrm{L}}(\omega)G^{\mathrm{a}}(\omega) + \frac{2k_{\mathrm{B}}T_{\mathrm{R}}}{\pi}\int_0^{\infty} \mathrm{d}\omega\omega G^{\mathrm{r}}(\omega)\Gamma_{\mathrm{R}}(\omega)G^{\mathrm{a}}(\omega), \quad (8)$$

where T_{L} and T_{R} are the temperatures of the heat baths. Conventionally, we can use $J_{i\to j} = -\langle (K_{ji}x_i)\frac{p_j}{m_j}\rangle = -K_{ji}C_{ij}$ to calculate the site-to-site heat flux. However, to look into the spectrum-resolved details, we can define the phonon-spectrum-resolved correlation

$$C(\omega) = \frac{2k_{\mathrm{B}}\omega}{\pi}G^{\mathrm{r}}(\omega)[T_{\mathrm{L}}\Gamma_{\mathrm{L}}(\omega) + T_{\mathrm{R}}\Gamma_{\mathrm{R}}(\omega)]G^{\mathrm{a}}(\omega), \quad (9)$$

such that $C = \int_0^{\infty} \mathrm{d}\omega C(\omega)$. As such, we can calculate the spectrum-resolved heat flux $J_{i\to j}(\omega)$ from the i-th atom to the j-th atom as

$$J_{i\to j}(\omega) = -\left\langle (K_{ji}x_i)\frac{p_j}{m_j}\right\rangle = -K_{ji}C_{ij}(\omega). \quad (10)$$

By integrating over certain frequency range $[\omega_1, \omega_2]$, we can calculate the phononic heat flux contributed from this frequency range $[\omega_1, \omega_2]$,

$$J_{i\to j}(\omega_1, \omega_2) = \int_{\omega_1}^{\omega_2} \mathrm{d}\omega J(\omega) = -K_{ji}\int_{\omega_1}^{\omega_2} \mathrm{d}\omega C_{ij}(\omega). \quad (11)$$

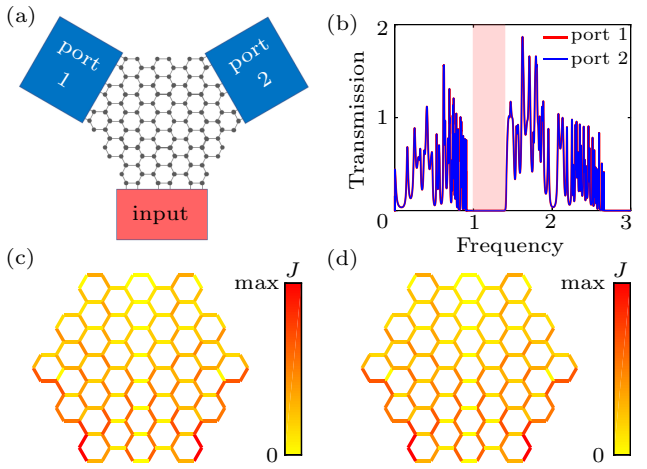


Fig. 2. (a) Diagram of thermal demultiplexer. The main body is constructed of finite honeycomb lattice with dangling atoms, but not draw up for convenience. One input port (red rectangle) and two output ports (blue rectangles) connect with the edge atoms. (b) Transmissions of ports 1 and 2 calculated by NEGF. They are identical due to the symmetry of the junction. The ENM zone is marked by pink shadow region. (c) Heat flux in low frequency range and the integral interval is [0, 1.25]. (d) Heat flux in high frequency range and the integral interval is [1.25, 5].

By using NEGF, it is straightforward to calculate the transmission from the input port to port 1 and port 2 shown in Fig. 2(b). We find that transmission to port 1 is the same as transmission to port 2. This is because there is only one kind of dangling atoms which keeps the symmetry of the junction. Besides, we can also calculate the heat flux by Eqs. (8), (11), and (10). In this work we use Langevin heat bath and the self-energy is $\Sigma_u^+(\omega) = \mathrm{i}\gamma\omega$, $u =$ input, port 1, port 2, $\gamma = 0.2$. The temperature of the input port is $T_{\mathrm{input}} = 1$ and the temperatures of ports 1 and 2 are $T_1 = T_2 = 0.6$. To visualize the transport of phonon, Fig. 2(c) shows the heat flux of every bond in the frequency range of acoustic branch [0, 1.25] while Fig. 2(d) shows the heat flux in the frequency range of optical branch [1.25, 5]. It is clear that the heat flux is also symmetric both in high and low frequency ranges, which is intuitive.

3. Results and discussion

In this section, we first study the two-mass thermal demultiplexer. To achieve a better performance, we use the four-mass thermal demultiplexer and genetic algorithm to optimize the configuration.

3.1. Two-mass configuration

Based on the above analysis, it is easy to tune the band gap by changing the dangling atoms' mass. Hence we can use this effect to realize a phonon demultiplexer. One of the designing methods is optimizing the distribution of dangling atoms with different mass to form several freqeuncy gaps, which can influence the phonon transport.

As for the configuration of dangling atoms, we first consider the equipartition configuration, which means each kind of dangling atoms only exists on one side. It is intuitive that phonons in different frequency ranges may split roughly and flow into different ports. The configuration of dangling atoms is shown in Fig. 3(a). The lattice atoms ($m_0 = 1$) with dangling atom mass $m_1 = 0.5$ are on the left part, marked by red and those with dangling atom mass $m_2 = 2$ are on the right part, marked by blue.

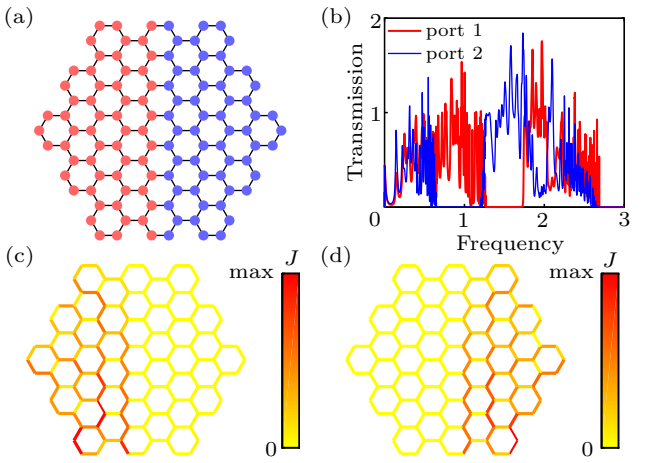


Fig. 3. (a) Schematic view of sites configuration with equipartition of dangling atoms. The sites with dangling atom mass 0.5 are colored as red, while the sites with dangling atom mass 2 are colored as blue. (b) Transmission of equipartition configuration which shows that different mass of dangling atoms will contribute different frequency gap. (c) Heat flux in low frequency range [0.66, 1.25]. In this frequency range, the heat flux will mainly flow into port 1. (d) Heat flux in high frequency range [1.25, 1.70]. In this frequency range, the heat flux will mainly flow into port 2. In these two frequency ranges, the heat flux and phonons have been split completely, while in the other frequency range the heat flux does not split completely.

The transmission is shown in Fig. 3(b), which can be calculated by NEGF method. It illustrates that transmission of port 1 in frequency range [0.66, 1.25] is much larger than the transmission of port 2. While in another frequency range [1.25, 1.70], the result reverses. This result demonstrates that in equipartition configuration the transmission of one port will be largely affected by dangling atoms of its side. We also plot the heat flux calculated by Eq. (10) in Figs. 3(c) and 3(d). Figure 3(c) shows the heat flux in low frequency range and the integral interval is [0.66, 1.25]; while Fig. 3(d) shows the heat flux in high frequency range and the integral interval is [1.25, 1.70]. The reason we choose these two intervals is that phonons in these two frequency ranges split quite completely. To show the degree of splitting, we define α as

$$\alpha = \frac{J_{\max}}{J_{\min}}, \tag{12}$$

where $J_{\max}$ and $J_{\min}$ are the maximum and minimum values of the two ports' heat flux in the same frequency range. After defining the rate α, it is easy to calculate that $\alpha_{\rm l} = 37.3$ in low frequency range [0.66, 1.25] and $\alpha_{\rm h} = 253.2$ in high frequency range [1.25, 1.70].

3.2. Four-mass configuration and genetic algorithm optimization

Although equipartition configuration of two masses can split phonons in certain frequency range, it is still possible to broaden the splitting frequency range and enhance its performance. To reach this goal, we introduce four kinds of dangling atoms. We choose four different dangling atom masses: $m_1 = 0.5$ (red), $m_2 = 2$ (blue), $m_3 = 0.2$ (black), and $m_4 = 5$ (green). We first calculate the transmission of equipartition configuration shown in Fig. 4(a). From the transmission Fig. 4(b), we find that the splitting effect does not get better. Then we choose a random configuration shown in Fig. 4(c) and calculate the transmission shown in Fig. 4(d). Compared with transmission of equipartition configuration, the splitting frequency range broadens. Then we attempt to find the best configuration. Thus, we perform the GA to optimize the configuration.

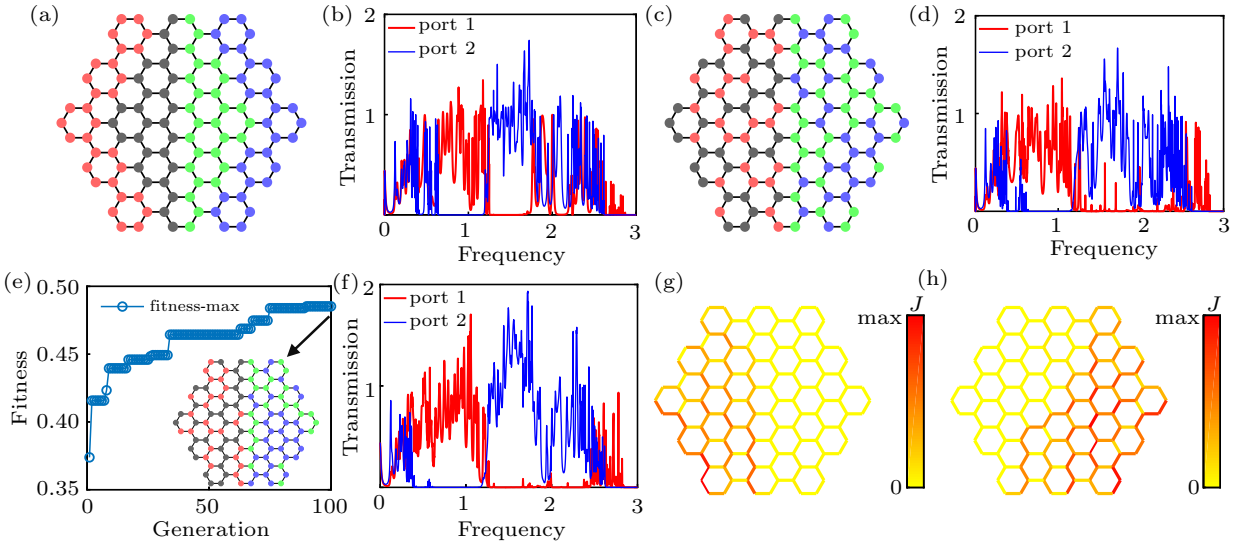


Fig. 4. (a) Schematic view of equipartition configuration of dangling atoms and their masses are 0.2 (black), 0.5 (red), 2 (blue), and 5 (green), respectively. (b) Transmission of equipartition configuration. (c) Diagram of random configuration which is one of the initial configurations of GA optimization. (d) Transmission of random configuration which broadens the splitting frequency range. (e) Optimization curve and the inset is the final optimal configuration. (f) Transmission of the final optimal configuration. (g) Real space profile of heat flux in low frequency range [0.40, 1.25]. (h) Real space profile of heat flux in high frequency range [1.25, 2.45]. The splitting frequency ranges are expanded larger and clearer. The heat flux in the lower frequency range will almost completely flow into the left port, while the heat flux in the higher frequency range will almost completely flow into the right port.

Machine learning has attracted lots of interest due to its efficiency of dealing with complex problem in the area of photonics,[38] phononics,[39] etc. GA is the one that can solve the problem of finding extreme value.[40,41]

The explicit process of GA is described as follows: (1) define the fitness to represent how close the result is to the optimization objective, (2) initialize the population containing dozens of genotypes (various configurations in this paper), (3) calculate fitness, (4) choose a few of the highest fitness configurations to create a new population by crossover and mutation, (5) repeat (2)–(4) for generations. An appropriate fitness function is essential to GA. Our objective is to split the phonons with different frequencies, thus it is necessary to enlarge the transmission difference of two ports in a certain frequency region. Therefore we define fitness function F as

$$F = \int_0^\infty f(\omega)\,\mathrm{d}\omega, \tag{13}$$

$$f(\omega) = \begin{cases} \mathcal{T}_1(\omega) - \mathcal{T}_2(\omega), & \omega < \omega_{\rm c} \\ \mathcal{T}_2(\omega) - \mathcal{T}_1(\omega), & \omega \geqslant \omega_{\rm c}, \end{cases} \tag{14}$$

where $\mathcal{T}_1$ and $\mathcal{T}_2$ are the transmissions from the input port to port 1 and port 2, respectively. $\omega_{\rm c}$ is the critical frequency that

we want to split the phonons and we set $\omega_c = 1.25$ here. The number of population is 30 and optimization will evolve for 100 generations.

We plot the maximum fitness of every generation as the optimization curve shown in Fig. 4(e) and the inset is the optimal configuration. The transmission is calculated and shown in Fig. 4(f). It is obvious that the optimal configuration works well in broader frequency range [0.40, 2.45]. Then we calculate the heat flux of two frequency ranges [0.40, 1.25] and [1.25, 2.45] shown in Figs. 4(g) and 4(h), respectively. And the splitting rate $\alpha_l = 51.7$ and $\alpha_h = 125.6$, which implies a good splitting effect.

Finally, we give a qualitative explanation of the optimization result. We have the knowledge that the certain mass of dangling atoms will cause the certain frequency gap so that we need different masses of dangling atoms to broaden the frequency gap. Besides, compared with the equipartition configuration, disorder in random and optimal configurations will merge the frequency gaps induced by different masses of dangling atoms. For these two reasons, the optimal configuration has much better performance. Furthermore, as for an atom whose $m \sim 10^{-26}$–10^{-27} kg and $a \sim 1$ Å, it yields the unit of physical frequency $(k/m)^{1/2} \sim 10^{13}$ Hz.

There is still a key problem remaining to be solved in our work that the thermal demultiplexer cannot work in a low frequency range. This is mainly because vibration of low frequency cannot be influenced by localized mode no matter which mass we choose. And even for the heterogeneous onsite potential, it will suppress the phonon transmission in the low frequency range but will not solve the problem completely since the transmission in low frequency range will shift to higher frequency range, which makes it still difficult to distinguish the transmissions of two ports. Another thing that can be improved is the splitting rate α since we find the α of low frequency range is quite smaller than the high frequency one. We are going to reveal it in future work.

4. Conclusion

In summary, we have proposed the thermal demultiplexer, which selectively transmits phonons of different frequencies to different ports. This is achieved by exploiting the effective negative masses caused by dangling atoms to induce frequency gaps. By constructing a three-port device, we have calculated the phonon transmission and spectrum-resolved heat flux of a two-mass configuration, which shows phonons splitting in frequencies at different ports. To broaden the phonon splitting frequency range, we have further chosen four kinds of masses and used genetic algorithm to optimize the configuration of dangling atoms for a better performance. Our study finds a way to selectively split spectrum-resolved phonons to different ports, which would provide a new means to manipulate phonons and guide the design of phononic devices in the future.

References

[1] Li N B, Ren J, Wang L, Zhang G, Hanggi P and Li B W 2012 *Rev. Mod. Phys.* **84** 1045
[2] Hu R, Iwamoto S, Feng L, Ju S H, Hu S Q, Ohnishi M, Nagai N, Hirakawa and Shiomi J 2020 *Phys. Rev. X* **10** 021050
[3] Chakraborty P, Liu Y, Ma T, Guo X, Cao L, Hu R and Wang Y 2020 *ACS Appl. Mater. Interfaces* **12** 8795
[4] Ju S H, Shiga T, Feng L, Hou Z F, Tsuda K and Shiomi J 2017 *Phys. Rev. X* **7** 021024
[5] Yamawaki M, Ohnishi M, Ju S H and Shiomi J 2018 *Sci. Adv.* **4** eaar4192
[6] Yang N, Ni X X, Jiang J X and Li B W 2012 *Appl. Phys. Lett.* **100** 093107
[7] Song Q C, An M, Chen X D, Peng Z, Zang J F and Yang N 2016 *Nanoscale* **8** 14943
[8] Ma D K, Wan X and Yang N 2018 *Phys. Rev. B* **98** 245420
[9] Chen S S, Wu Q Z, Mishra C, Kang J Y, Zhang H J, Cho K J, Cai W W, Balandin A A and Ruoff R S 2012 *Nat. Mater.* **11** 203
[10] Maire J, Anufriev R, Yanagisawa R, Ramiere A, Volz S and Nomura M 2017 *Sci. Adv.* **3** e1700027
[11] Zhai J X, Zhang Q Y, Cheng Z H, Ren J, Ke Y Q and Li B W 2019 *Phys. Rev. B* **99** 195429
[12] Evans W J, Hu L and Keblinski P 2010 *Appl. Phys. Lett.* **96** 203112
[13] Li B W, Wang L and Casati G 2004 *Phys. Rev. Lett.* **93** 184301
[14] Ren J and Zhu J X 2013 *Phys. Rev. B* **87** 241412(R)
[15] Li B W, Wang L and Casati G 2006 *Appl. Phys. Lett.* **88** 143501
[16] Joulain K, Drevillon J, Ezzahri Y and Ordonez-Miranda J 2016 *Phys. Rev. Lett.* **116** 200601
[17] Wang L and Li B W 2008 *Phys. Rev. Lett.* **101** 267203
[18] Li S, Ding X D, Ren J, Moya M, Li J, Sun J and Salje E K H 2014 *Sci. Rep.* **4** 6375
[19] Wang L and Li B W 2007 *Phys. Rev. Lett.* **99** 177208
[20] Han H, Li B W, Volz S and Kosevich Y A 2015 *Phys. Rev. Lett.* **114** 145501
[21] Chang C W, Okawa D, Majumdar A and Zettl A 2006 *Science* **314** 1121
[22] Giazotto F and Martinez-Perez M J 2012 *Nature* **492** 401
[23] Ito K, Nishikawa K, Iizuka H and Toshiyoshi H 2014 *Appl. Phys. Lett.* **105** 253503
[24] Su L, Piggott A Y, Sapra N V, Petykiewicz J and Vuckovic J 2017 *ACS Photon.* **5** 301
[25] Piggott A Y, Lu J, Lagoudakis K G, Petykiewicz J, Babinec T M and Vuckovic J 2015 *Nat. Photon.* **9** 374
[26] Faiz M S, Addouche M, Zain A R M, Siow K S, Chaalane A and Khelif A 2020 *Appl. Sci.* **10** 4594
[27] Moradi P and Bahrami A 2019 *Chin. J. Phys.* **59** 291
[28] Rostami-Dogolsara B, Moravvej-Farshi M K and Nazari F 2016 *IEEE Trans. Ultrason. Ferroelectr. Freq. Control* **63** 1468
[29] Liu X N, Hu G K, Sun C T and Huang G L 2011 *J. Sound Vib.* **330** 2536
[30] Liu X N and Hu G K and Vestnik S 2016 *J. Mech. Eng.* **62** 403
[31] Wang Y F, Wang Y Z, Wu B, Chen W Q and Wang Y S 2020 *Appl. Mech. Rev.* **72** 040801
[32] Zhang D M, Ren J, Zhou T X and Li B W 2019 *New J. Phys.* **21** 093033
[33] Yao S S, Zhou X M and Hu G K 2008 *New J. Phys.* **10** 043020
[34] Wang J S, Wang J and Lu J T 2008 *Eur. Phys. Jour. B* **62** 381
[35] Wang J S, Agarwalla B K, Li H N and Thingna J 2014 *Front. Phys.* **9** 673
[36] Dhar A and Roy A J 2006 *Stat. Phys.* **125** 805
[37] Dhar A 2008 *Adv. Phys.* **57** 457
[38] Long Y, Ren J, Li Y H and Chen H 2019 *Appl. Phys. Lett.* **114** 181105
[39] Long Y, Ren J and Chen H 2020 *Phys. Rev. Lett.* **124** 185501
[40] Wang Y and Ren J 2020 *Phys. Chem. Chem. Phys.* **22** 4481
[41] Gao Z B, Dong X, Li N B and Ren J 2017 *Nano Lett.* **17** 772